Examining Land Surface Temperature Relations with Major Air Pollutant: A Remote Sensing Research in Case of Tehran

Kamyar Fuladlu
Eastern Mediterranean University: Dogu Akdeniz Universitesi
Hasim Altan (hasimaltan@gmail.com)
Arkin University of Creative Arts and Design (ARUCAD) https://orcid.org/0000-0002-9534-1961

Research

Keywords: Land Surface Temperature, Major Air Pollutants, Sentinel-3 SLSTR, Sentinel-5 Precursor, Tehran

Posted Date: March 12th, 2021

DOI: https://doi.org/10.21203/rs.3.rs-281262/v1

Version of Record: A version of this preprint was published at Urban Climate on August 23rd, 2021. See the published version at https://doi.org/10.1016/j.uclim.2021.100958.

Examining Land Surface Temperature Relations to Major Air Pollutant: A Remote Sensing Research in Case of Tehran

Kamyar FULADLU[a], Haşim ALTAN*[b]

a. *Faculty of Architecture, Department of Architecture, Eastern Mediterranean University, Famagusta, 99628, Cyprus*

b. *Faculty of Design, Department of Architecture, Arkin University of Creative Arts and Design, Kyrenia, 99300, Cyprus*

Abstract:

Background. Urban air pollution is a multifaceted and dynamic mixture of Land Surface Temperature (LST), gaseous pollutants, and particulate matter with daily and seasonal changes due to anthropogenic activities, land-cover transformation, and climatic conditions. Today, the relationship between urban biophysical and thermal conditions and their relationship with land-cover is well-known. However, the absence of a dense network of land-based meteorological stations was an obstacle to the study of LST in comparison to the Major Air Pollutant (MAP).

Method. The current research proposes an integration of LST derived by Sentinel-3 SLSTR, to investigate LST relationships to the MAP derived by Sentinel-5 Precursor, and air pollution monitoring system station of Iran in the case of Tehran province. The method of research is designed in a time-series manner with the use of a Python application programming interface, geographical information system, and remote sensing.

Result. Based on the mean concentration of the Particular Matter (PM), Sulfur dioxide (SO_2), and Nitrogen dioxide (NO_2) are mainly in the Tehran metropolis and the core of the urban area. A negative correlation was noted between the PM_{25}, SO_2, NO_2, and altitude, additionally, increasing the altitude negatively affects the concentration of the LST, Carbon monoxide (CO), and Ozone (O_3) values in Tehran province. Unlike, CO and O_3 have positive correlations with LST, which stand for the mutual impacts of the LST, CO, and O_3 values in Tehran province.

Keywords: Land Surface Temperature; Major Air Pollutants; Sentinel-3 SLSTR; Sentinel-5 Precursor; Tehran

1. Introduction

Urban warming and the formation of Urban Heat Island (UHI) is one of the features of land transformation, which is of interest to the disciplines because the UHI indicates a wide range of changes in the earth's surface that affect human health, ecosystem, local-weather and, possibly climate (Fuladlu, Riza, & İlkan, 2018a). Dominantly the potential of the urban area increases the urban desire for the living of many people. Rapid urban population growth results in urban expansion and urban sprawl (Fuladlu, 2019, 2020; Fuladlu, Riza, & İlkan, 2018b), and encroachment on limited agricultural and green areas leading to the destruction of green-cover. This destruction, along with population growth, causes environmental effects such as rising Land Surface Temperature (LST), UHI, and air pollution. LST is considered a significant parameter in the formation of urban climate. LST is directly related to the canopy layer of UHI, and LST closely corresponds to the land-cover (See Feizizadeh & Blaschke, 2013; Fu & Weng, 2016; Weng, 2009; Weng, Lu, & Schubring, 2004; Weng & Yang, 2006).

LST research indicates that the energy balance of the earth's surface can be affected by surface soil conversion, water content, and vegetation. It is well-known that the input and output radiation of urban surfaces corresponds to the

* *Corresponding author email address: hasimaltan@gmail.com*

distribution of land-cover properties (Owen, Carlson, & Gillies, 1998). The association between Major Air Pollutant (MAP) and LST (and therefore UHI) is not clearly understood, although both relate to urban land-cover. Although UHI's assists the development of MAP, but not an indicator of MAP. Additionally, higher urban temperatures stand for energy use, mainly due to higher demand for air conditioning. As power plants burn more fossil fuels, pollution levels increase (Weng & Yang, 2006). MAP includes Sulfur dioxide (SO_2), Nitrogen dioxide (NO_2), Carbon monoxide (CO), Particular Matter (PM), lead (Pb), and Ozone (O_3), which are frequently used as indicators of air pollutants in ambient air. According to the European Union Council Directive 96/62/EC, MAPs are target species due to their negative impact on human health and vegetation (Fenger, 1999; Flemming, Stern, & Yamartino, 2005; Wiederkehr & Yoon, 1998; Zabalza et al., 2007).

SO_2 and NO_2 have anthropogenic and natural sources, the majority are produced from fossil fuel combustion (Brunelli, Piazza, Pignato, Sorbello, & Vitabile, 2007; Krotkov et al., 2016; Weng & Yang, 2006). Both are short-lived trace gases that have key roles in tropospheric chemistry. Major sources of NO_x (NO_x=NO+NO_2) includes fossil fuel combustion, mediated biomass burning, industrial and transportation emissions, and lightning (Krotkov et al., 2016; Xue et al., 2020). NO_2 affects atmospheric oxidation rates participating in the formation of surface ozone (Krotkov et al., 2016; Meng et al., 2008). The natural source of SO_2 is volcanic eruptions, which can release a large amount of SO_2 above the Planetary Boundary Layer (PBL). The anthropogenic source of SO_2 was burning sulfur-contaminated fossil fuels and the refinement of sulfide ores, which were mainly concentrated in the PBL (Krotkov et al., 2016; Xue et al., 2020). CO is emitted in urban areas by motor-vehicle traffic, and reducing traffic speeds may increase CO emissions. Therefore, the catalytic converter contributes to the reduction of CO diffusion by combining oxygen, CO, and unburned hydrocarbons to produce carbon dioxide and water (Brunelli et al., 2007; Fenger, 1999).

Institutional PM is not quite clear but is designated as soot or black smoke, the major part of PM_{10} may have a natural origin, therefore important to measure PM_{25}. Ventilation change has stronger effects on PM concentrations typically decrease by an order of magnitude between polluted regions and the diluting background air. PM concentration decreases with increasing precipitation because wet deposition results in the main PM sink. Thin dust consists of particles between 0.005 and 100 µm in diameter (Fenger, 1999; Jacob & Winner, 2009). Thin dust is composed of particles between 0.005 and 100 µm in diameter. In particular, the PM_{10} class, which contains particles less than 10 µm in diameter, is receiving legal and scientific attention for its effects on human health. They are formed by a wide variety of solids and liquids substances from natural resources or human activities such as central heating, industry, vehicle traffic, home heating, and industrial incinerators. Particles with a diameter of less than 10 µm, the so-called inhalable fraction, are able to reach the bronchopulmonary region. Particles less than 2.5 µm in diameter, which make up the breathable part, can reach the alveoli of the lungs and form all of their constituents in living matter (Brunelli et al., 2007).

O_3 is a bluish toxic gas made up of unstable molecules, it is an energetic oxidant that is capable of degrading organic and inorganic material. O_3 is low in concentrations at the troposphere and represents a particularly insidious secondary pollutant. By examining the diurnal cycles of O_3 from the typical stations that are heavily influenced by motor-vehicle traffic, a maximum specified in the afternoon due to the formation of photochemical O_3 and the relatively low secondary maximum were recorded in the early morning, which seems to be the result of downward transport of O_3 from higher-level containing more O_3. Besides O_3 concentrations are higher in the hottest months of the year due to severe insulation, high pressure, and low ventilation along with stagnation and accumulation of pollutants (Brunelli et al., 2007; Mayer, 1999).

Today relation of urban biophysical and thermal conditions, as well as their relation to land-cover, are well-known. However, the absence of a dense network of land-based meteorological stations was an obstacle for the examination of

LST in comparison to the MAP. Likewise, land-based stations can be monitoring near-surface concentrations of trace gases with limited spatial information (Xue et al., 2020). Hence studies for examination of LST in comparison to the MAP were not forwarding. However, some studies were published with those limitations. For instance, Weng and Yang (2006) in the case of Guangzhou City in South China, by use of the Geographic Information System (GIS) approach, tried to examine the spatial pattern of air pollution and land use. Results depict that the spatial patterns of air pollutants probed were positively correlated with urban built-up density. Feizizadeh and Blaschke (2013) in the case of Tabriz city in Iran found a correlation between land-cover, land surface temperature, and air pollutants. The main objection to the above-mentioned studies is that they are both based on one or two points in time, which significantly reduces the accuracy of the pollutants study. Therefore, to achieve a reliable research, it is better to use several time points instead of one or two points in time.

Consequently, instead of a specific point in time, the time-series method recorded certain variables in a particular place that is related to evolution over time. Time-series take place in a wide range of phenomena, from economics to the physical sciences, and general methods may be applied without the need for prior knowledge of the fundamental causal links between dependent and independent variables (Salcedo, Alvim-Ferraz, Alves, & Martins, 1999). For instance, air quality monitoring is a good example of an environmental time-series study. The method commonly used to estimate environmental parameters is based on classical descriptive statistics, but due to the high variability associated with air quality data and the low signal-to-tonnage ratio of existing measurements, this value is relatively limited. Accordingly, time-series studies may be a good tactic to avoid these difficulties by agreeing to the identification of hidden deterministic behavior and thus contributing to an understanding of origin and consequence associations in environmental and urban problems (Schwartz & Marcus, 1990).

According to the given introduction, until a few years ago monitoring air pollutants from a satellite was not easy as today, and most studies are limited to land-based meteorological stations. However, the Sentinel-5 Precursor satellite was successfully launched on 13 October 2017 from the Plesetsk Cosmodrome in Russia, and scenes partially were released on 10 July 2018. The Sentinel-5 Precursor is a successful step towards observing air pollutants from the satellite. Therefore, research like the current one become applicable for monitoring air pollutants with the use of remote sensing and GIS. The current research proposes an integration of LST derived by Sentinel-3 SLSTR, to investigate LST relationships to the MAP derived by Sentinel-5 Precursor, and Air Pollution Monitoring System (APMS) land-based station of Iran in the case of Tehran province, which is consist of urban, suburban, and rural (Figure 1). The method of research is designed in a time-series manner with the use of Python (Application Programming Interface) API, GIS, remote sensing, and various statistics including regression and correlation have been integrated.

2. Case Study and Methods

2.1. Case Study

Ťehrân (Figure 1; 35°41′21″N, 51°23′20″E) province is the capital of Iran, Tehran province with a population of around 25 million people, about 9 million people live in the metropolis of Tehran and the rest live in other cities of Tehran province. According to the shape-file, Tehran metropolis has an area of about 2,129 Km² and 26,880 Km² is rest of the province. The population density of the Tehran province was reported as about 11,800 Km². Tehran province is the most populous city in Iran and Western-Asia and has the 2nd largest metropolitan area in the Middle-East after Cairo. This province is ranked 24th in the world according to the population of the world's metropolises. The metropolis of Tehran is divided into 22 municipal districts, each with its administrative center. 20 of the 22 municipal districts are located in the

metropolis of Tehran, while the districts number 1 and 20 are respectively located in the counties of Shemiran and Ray. Although administratively separate, the cities of Shemiran and Ray are often considered part of Tehran province.

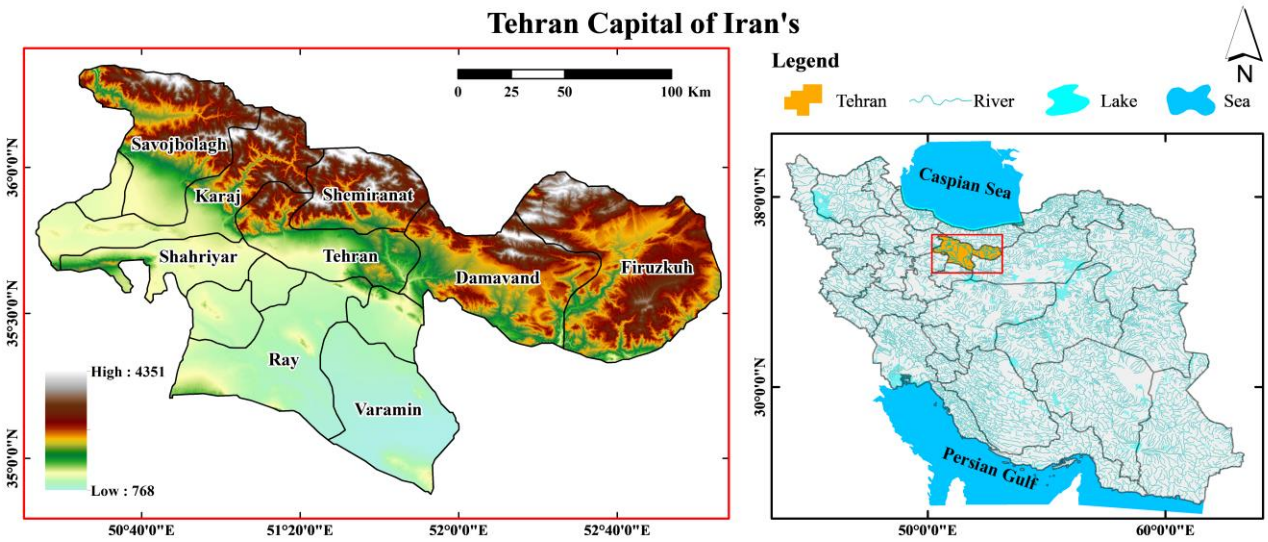

Figure 1. Case Study of Tehran Province DEM (left) Iran (right)

Tehran province has a cold semi-arid climate with continental climate characteristics and a Mediterranean climate precipitation pattern. The climate is largely defined by its geographic location, with the towering Alborz Mountains to its north and the country's central desert to the south. It can be generally described as mild in spring and autumn, hot and dry in summer, and cold and wet in winter. Since the province has covered a large area, with significant differences in elevation among various cities and districts, the weather is often cooler in the hilly north than in the flat southern part of Tehran province. Summer is long, hot, and dry with little rain, but relative humidity is generally low, making the heat tolerable. Average high temperatures are between 32 to 37 °C, and it can occasionally drop to 14 °C in the mountainous north of the province at night. Most of the light annual precipitation occurs from late autumn to mid-spring, but none of these months have different humidity. July is usually the hottest month of the year, with a mean minimum temperature of 26 °C and a mean maximum temperature of 34 °C, and January is usually the coldest month of the year, with a mean minimum temperature of -5 °C and a mean maximum temperature of 1 °C. Based on some reports, the prevailing wind is from 270° with a mean speed of 5.5 m/s. At night, a cool breeze called Tochal breeze blows down from the mountain, and on the contrary, during the day a breeze blows from the plain.

The metropolis of Tehran suffers from severe air pollution, it can be stated that about 80 percent of pollution is caused by cars and the rest is emitted by industries that are mostly located on the border of the metropolis. Other estimates suggest that motorcycles alone account for 30 percent of Tehran's air pollution and 50 percent of its noise pollution. Likewise, Tehran metropolis is known as an important source of greenhouse gas emissions in the Middle-East. During recent years due to environmental issues in the Tehran metropolis, different plans to relocate the capital have been discussed over and over again. For instance, in 2010, the government announced that, for various reasons, the plan to move the capital from Tehran was being finalized. The government is planning to transfer about 163 state-owned companies and several universities from Tehran. But this plan has never been implemented after a decade. In recent years, the government has made great efforts to reduce air pollution. For instance, it has encouraged taxi and bus drivers to switch to compressed natural gas as a fuel that can be used in place of gasoline, diesel fuel, and liquefied petroleum gas. Besides, the government has created several traffic zones that cover metropolis centers during peak hours. In these traffic areas, cars are allowed to enter only with a special permit. Besides, there are also different programs to raise public

awareness of the dangers of pollution. The method used is to install pollution indicator signs in the metropolis to control the levels of PM_{25}, SO_2, NO_2, CO, and O_3.

2.2. Methods

The current research, to design its time-series for the case of Tehran province chose a period between January 2020 to December 2020, a period of one year, which is good enough to present hot to cold months of the year. Accordingly, with the above specified period, twelve senses were obtained from the Sentinel-3 SLSTR and forty-eight senses from the Sentinel-5 Precursor satellite from the first day of each month to represents a point in time. The required values as a big-dataset include latitude, longitude, unit, fill-value, LST, SO_2, NO_2, CO, and O_3 columns with the use of the Python API, which was extracted from the NetCDF4 datasets and was re-casted in the rasters format. In the continuation of the process, the fill-value is replaced by the No-Data to eliminate the process bias. The Model-Builder of GIS was used to manage the workflows and sequences of geoprocessing including clip, re-projection, rastering, classification, and spatial join. Similarly, all the required pixels were extracted from the Tehran level-2 boundary shape-file, and to avoid distortion, rasters were transferred to the WGS84 UTM Zone 39 North projections. Finally, all rasters generated a dataset for the current research and classified by Jenks' natural breaks method.

Since Sentinel satellites are not covered the PM value, the PM values with 2.5 µm directly integrated with the use of the APMS land-based station of Iran into the research. Accordingly, the required values for a similar period with the use of Python API from the APMS website were acquired and save as JSON files. All the JSON datasets were cleaned and after that converted to the CSV file extension. Consequently, CSV extension files joined to the relevant station's longitude and latitude regarding the Open Street Map on the EPSG:4326 projections. The Inverse Distance Weighted (IDW) interpolation function of GIS was used to rasterize the CSV datasets. The IDW interpolation determines cell values using a linearly weighted combination of a set of sample points. Accordingly, the weight is a function of inverse distance, the surface being interpolated should be that of a locationally dependent variable. This function assumes that the variable being mapped decreases in influence with distance from its sampled location. One kilometer cell size experimentally and similar to the Sentinel-3 SLSTR resolution were chosen for output of IDW and an overall result was extracted from the Tehran level-2 boundary shape-file.

As mentioned earlier, the geographical elevation of Tehran province significantly changes from north to south. Likewise, the north part is hilly and the south part is almost flat. Since altitude is an effective factor for the study of LST and MAP, therefore the current research integrates the Tehran Digital Elevation Model (DEM) into the research. Accordingly, the ASTER Global DEM satellite was used for developing the Tehran DEM dataset. Likewise, it required senses regarding the Tehran level-2 boundary, which were acquired from ASTER Global DEM satellite and mosaicking into a unique raster. The Tehran province DEM is integrated and exposed in Figure 1. The resolution of the ASTER Global DEM satellite is thirty meters, and the resolution of the Sentinel-3 SLSTR and IDW is one kilometer while the resolution of the Sentinel-5 Precursor satellite is four and a half kilometers. There are several methods for matching or extracting pixel values from senses with different resolutions; each method has advantages and disadvantages. Some studies prefer sense-to-sense registration and re-sample senses regarding the last sense in time (Richards & Jia, 1999, p. 57). However, the current research experimentally used Honeycombs (Hexagonal grids) tessellation. Honeycomb has some benefits in comparison to the Fishnet (Square grids) such as reduced edge effects, all neighbors are identical, better fit to curved surfaces, and a honeycomb look way more impressive.

Accordingly, a honeycomb tessellation shape-file in GIS was created regarding the Tehran province boundary. The side of the honeycomb was 1.15 Km and the area is about 3.44 Km^2, which is equal to the mean of all three satellites' area

resolution, likewise 8,814 honeycombs enough for covering the Tehran province boundary accurately. Subsequently, the mean of each six datasets for LST, PM_{25}, SO_2, NO_2, CO, and O_3 will be calculated from the relevant rasters. During the process no-data and null-data pixels will be eliminated from the mean calculation; the calculation of the mean value done through the interpolate function for each dataset. Accordingly, five unique rasters will be created which are representing the one year of this research. Eventually, to developed the honeycomb attributes (DEM, LST, PM_{25}, SO_2, NO_2, CO, and O_3), all calculated rasters together with DEM raster will be overlaid into the honeycomb. Likewise, all the extreme values', which are driven from the satellite noise, and values at the edge of the rasters will be eliminated as a bias from the honeycomb. To represent the honeycomb attributes Jenks' natural breaks will be used to classify the values into five classes of Low (blue), Medium-Low (green), Medium (yellow), Medium-high (orange), and High (red), and the results are exposed in Figure 2.

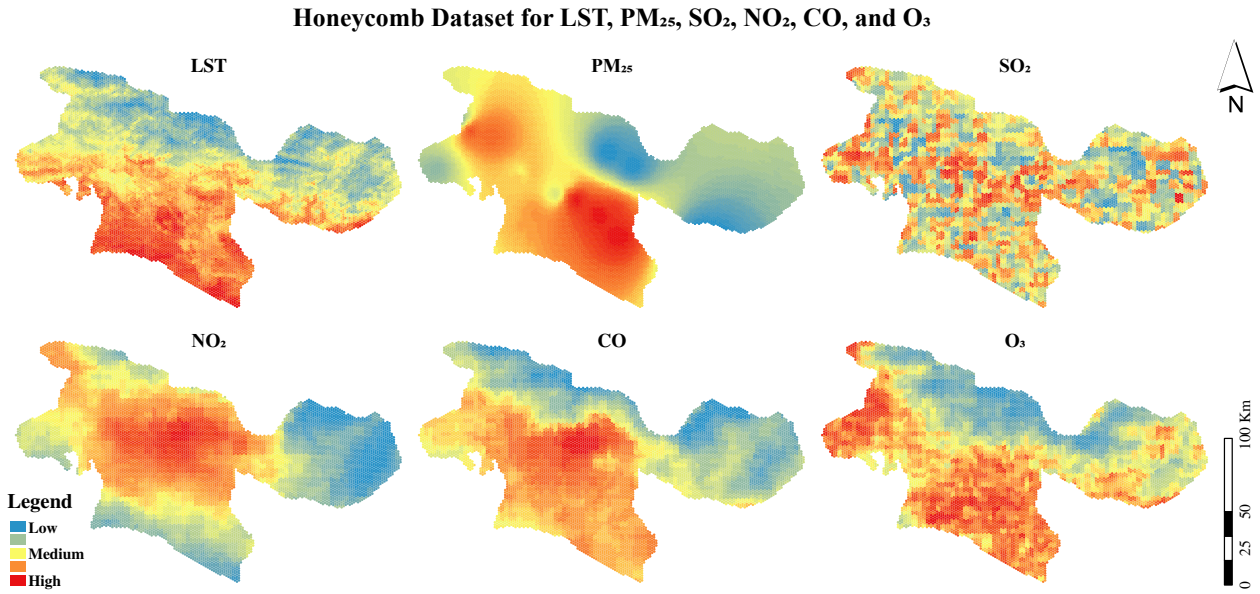

Figure 2. The Classified Honeycomb Attributes for LST, PM_{25}, SO_2, NO_2, CO, and O_3

Regarding the outcomes, the range of the MAP was as follows; PM_{25} from 60.9 to 93.8 µg/m³, NO_2 from 205×10^{-7} to 112×10^{-5} mol/m², SO_2 from 129×10^{-3} to 134×10^{-5} mol/m², CO from 200×10^{-4} to 422×10^{-4} mol/m², and O_3 from -141×10^{-5} to 176×10^{-5} mol/m². Likewise, the range value of the LST was from 273 to 302 kelvins. To quantify the outcomes, honeycomb attributes will be exported into the SPSS. Accordingly, DEM, LST, and PM_{25} were chosen as independent variables whereas SO_2, NO_2, CO, and O_3 are considered as dependent variables. Consequently, the following fifteen scatter-plots include trend lines are drawn among the variables for visualization and statistical comparisons (Figure 3).

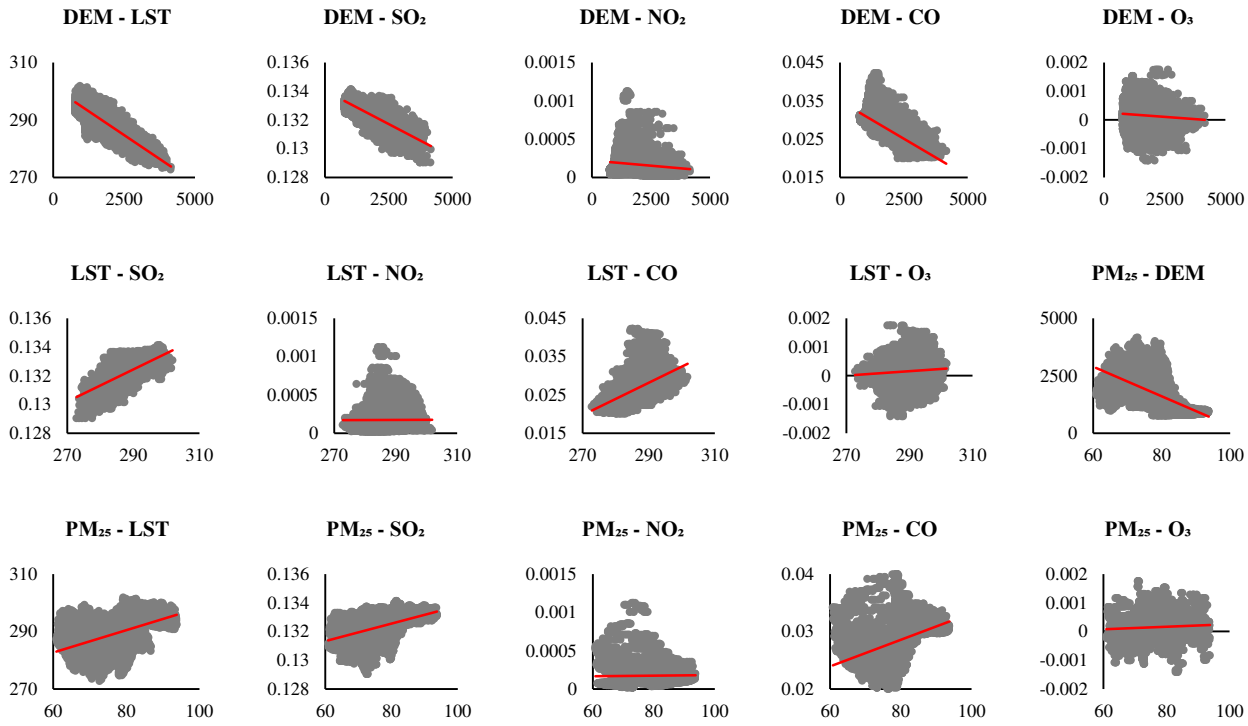

Figure 3. The Scatter-plot among the DEM, LST, PM_{25}, SO_2, NO_2, CO, and O_3

Additionally, from the honeycomb attributes a Pearson correlation with two-tailed significantly performed among the DEM, LST, PM_{25}, SO_2, NO_2, CO, and O_3, and the result are exposed in Table 1.

Table 1. Correlation Matrix among the DEM, LST, PM_{25}, SO_2, NO_2, CO, and O_3

		DEM	LST	SO_2	NO_2	CO	O_3	PM_{25}
DEM	Pearson Correlation	1						
	Sig. (two-tailed)							
LST	Pearson Correlation	**-.874****	1					
	Sig. (two-tailed)	0.000						
SO_2	Pearson Correlation	**-.116****	**.111****	1				
	Sig. (two-tailed)	0.000	0.000					
NO_2	Pearson Correlation	**-.145****	0.009	**.055****	1			
	Sig. (two-tailed)	0.000	0.407	0.000				
CO	Pearson Correlation	**-.789****	**.641****	**.108****	**.642****	1		
	Sig. (two-tailed)	0.000	0.000	0.000	0.000			
O_3	Pearson Correlation	**-.811****	**.744****	**.104****	**-.085****	**.539****	1	
	Sig. (two-tailed)	0.000	0.000	0.000	0.000	0.000		
PM_{25}	Pearson Correlation	**-.573****	**.457****	**.077****	0.015	**.416****	**.477****	1
	Sig. (two-tailed)	0.000	0.000	0.000	0.164	0.000	0.000	

**. Correlation is significant at the 0.01 level (two-tailed)

3. Results and Discussion

In this research, the LST, PM_{25}, SO_2, NO_2, CO, and O_3 values were obtained from the satellites and APMS land-based stations of Iran over Tehran province for a year. Consequently the mean of the values calculated within the boundaries of Tehran province and exposed as Figure 2. Based on the result (Figure 2) visually could be stated, the mean concentration of the PM_{25}, SO_2, and NO_2 are mainly in the Tehran metropolis and the core of the urban area, which could be attributed to the built density, population density, and central business district. Although, Table 1 depicts negative correlations between PM_{25}, SO_2, NO_2, and DEM, except for PM_{25} ($r=-.573$, $p<0.01$) partially both SO_2 ($r=-.116$, $p<0.01$) and NO_2 ($r=-.145$, $p<0.01$) are not significant in terms of correlation.

However, a comparison between Figure 1 (left) and Figure 2 depicts that the LST, CO, and O_3 values decreased by increasing the DEM values. In other words, increasing the altitude negatively affects the concentration of the LST, CO, and O_3 values in Tehran province. Additionally, Figure 3 depicts, increasing DEM result decay of LST, CO, and O_3 values. Furthermore, Table 1 could prove above mention statements since LST ($r=-.874$, $p<0.01$), CO ($r=-.789$, $p<0.01$), and O_3 ($r=-.811$, $p<0.01$) has negative correlations with DEM. Similarly, CO ($r=.641$, $p<0.01$) and O_3 ($r=.744$, $p<0.01$) has positive correlations with LST, which stand for the mutual impacts of the LST, CO, and O_3 values in Tehran province. This means increasing LST could be contributing to the accumulation of the CO and O_3 values. Besides, PM_{25} ($r=.457$, $p<0.01$) relatively has a positive correlation with LST. Of course, the PM_{25} value behavior in current research is partly influenced due to the different acquired method compared to the other values which are obtained from satellites. However, the current research tries to integrate the wind flow effect to figure out the wind flow impact on the PM_{25} concentration.

According to Figure 2, the concentration of PM_{25} mainly seen in the south, south-west, and slightly in the north-west and of Tehran province which could be attributed to the wind flow, Alborz mountains at north, and the central desert of the south. Since wind speed and wind direction significant impacts on the dispersion condition of the PM concentration (Nguyen, Park, & Lee, 2017; Zhang et al., 2018). Therefore, the metrology data include maximum wind speed and direction of the Tehran province according to the time-series of the research acquired in CSV format. Tehran province is covered by 16 synoptic stations, longitude, latitude, and altitude of the stations integrated with the dataset and IDW function of GIS were used for rasterizing. The wind-rose diagram with the use of Python API was created and exposed as Figure 4.

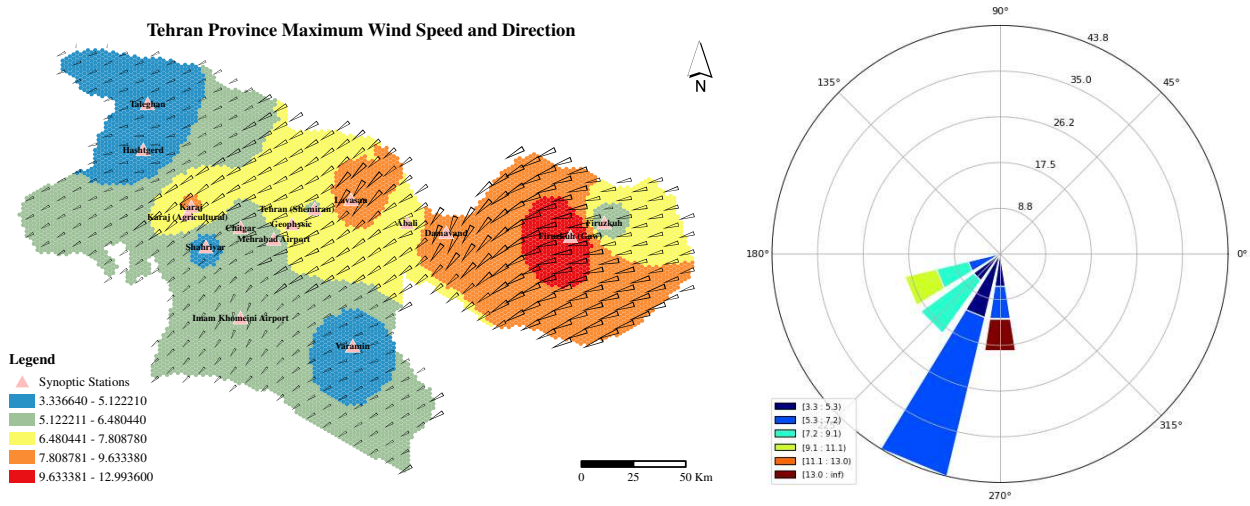

Figure 4. Synoptic Map of Tehran Province (left) Wind-rose diagram (right)

According to Figure 4, the winds are mainly flowing in the SSW direction with a maximum speed of 3.3 - 7.2 m/s. As stated early the Tehran province prevailing wind is in the S direction, where the PM_{25} concentration decrease in other place and mainly located at south and south-west of Tehran province. Likewise, a recent study identified fine PM concentrations gradually decreased with wind speed and direction while coarse PM concentrations may increase because of dust resuspension under strong wind (Nguyen et al., 2017; Zhang et al., 2018). Similarly, a negative correlation (Table 1 and Figure 3) seen between PM_{25} ($r=-.573$, $p<0.01$) and DEM value in Tehran province. To improve research perception min, mean, and max values plus trend line of LST, PM_{25}, SO_2, NO_2, CO, and O_3 in a monthly dataset accrued and developed following monthly line-plot (Figure 5). The following plots are useful for the monitoring variables during the years.

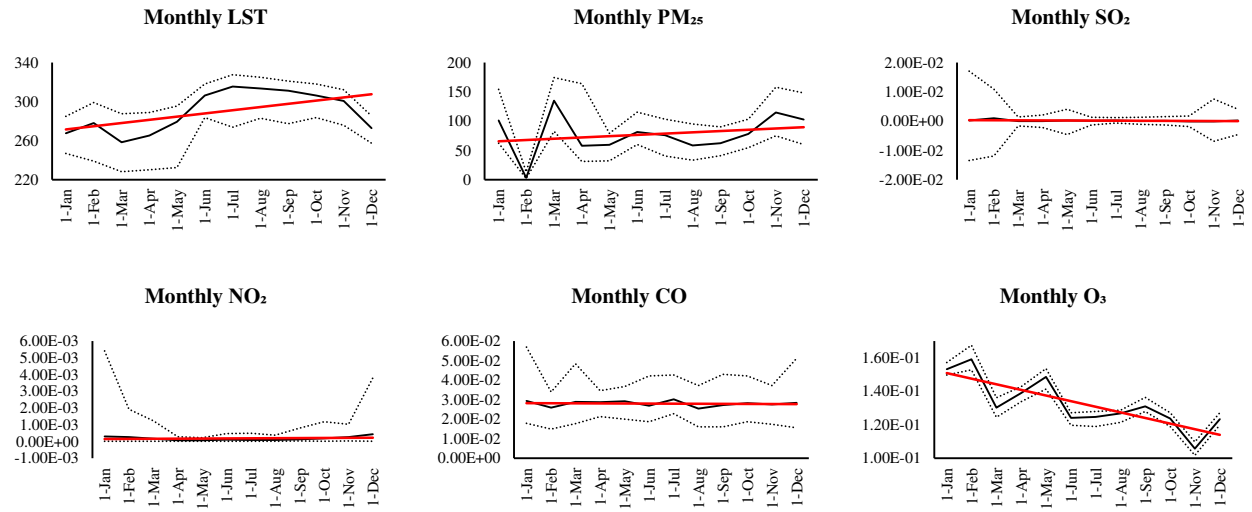

Figure 5. The Monthly Line-plot of the DEM, LST, PM_{25}, SO_2, NO_2, CO, and O_3

According to Figure 5 the LST, PM_{25}, and O_3 had the most fluctuation during the research year. Similarly, Figure 5 depicts the mean monthly value for the LST and PM_{25} are increasing from January 2020 to December 2020, which means that the LST and PM_{25} values are steadily increasing monthly during the research time. Unlike, the mean trend of SO_2, NO_2, and CO values remains almost unchanged during research periods. However, the O_3 values significantly decreased from the first of January 2020 till the first of December 2020. The alterations of the pollutant could be attributed to the atmospheric conditions and government policy. For instance, Dareshiri, Sahelgozin, Lotfian, and Ingensand (2019) study found that air pollution has decreased in the months with increased precipitation. Additionally, due to the pandemic COVID-19, forty-three days' quarantines policy from 21st November 2020 at 9:00 PM till 04:00 AM will be applied which includes traffic restriction to the Tehran metropolis. However, no noticeable change could be seen in any plots in Figure 5.

There is no doubt that the study of the alteration pollutant trends must be in line with existing policies at the same time. Although the study of government policies in this research is limited, it is recommended that subsequent studies simultaneously study the impact of government policies on the process of air pollutants. However, it could be confidently stated that research of this kind is significantly minimizing dependency on the census, statistical, temporal map, and census tract. Additionally, the combination of remote sensing and GIS like this research is recognized as a powerful and outstanding tool for monitoring alterations in the pattern of spatial distribution data (Weng, 2001, 2002). Relatedly, the method of current research could be performed cost-efficiently (Liu & Yang, 2015; Ridd, 1995) for monitoring and compearing the MAP and LST alteration. Since the core of the method developed based on the satellite data, which is compiled through the more than two-thousand satellites covering the planet.

4. Conclusions

Today, the effect of urban land-cover transformation on the formation of urban air pollution and the increase of MAP and LST has been confirmed. However, the relationship between MAP and LST is not clearly understood due to various mutual factors. To some extent, the study of MAP and LST also face related problems due to their dependence on the dense network of land-based meteorological stations. The current research with the use of remote sensing and GIS acknowledges the significant relation between LST (by its nature UHI) and MAP in the case of a research area. Additionally, the time-series method of this research proved the mean concentration of the PM, SO_2, and NO_2 is mainly in the Tehran metropolis and the core of the urban area. Besides, a negative correlation was noted between the PM_{25}, SO_2, NO_2, and DEM, likewise, increasing the DEM negatively affects the concentration of the LST, CO, and O_3 values in

Tehran province. Unlike, CO and O_3 have positive correlations with LST, which stand for the mutual impacts of the LST, CO, and O_3 values in Tehran province.

Since results indicate a significant positive correlation between UHI and MAP, this research believes that intensified UHI would stand for increased MAP and urban air pollution. Likewise, the result indicates the reputation of current research for decision-makers of the whole world and, in particular to policymakers of the Tehran province. Likewise, the current research provides a scientific approach and bases for future studies in monitoring the UHI and MAP instantly. The main advantage of the current method is monitoring both UHI and MAP with the use of remote sensing and GIS without limitation on the time and location of the studies. As stated before, current research limited to the available urban policies of the Tehran province, therefore highly recommended for future studies to integrate the existing policy of the study area within their research. Additionally, this research could be enriched by feeding through the other values from the land-based synoptic stations such as temperature, relative humidity, and barometric pressure.

Acknowledgments

The authors wish to acknowledge Arosha Architecture for providing synoptic data of the Tehran province. Besides, urban research development and technology for providing the resources and materials that supported the author's execution of this research.

Authors' contributions

The current research proposed the LST relationships to the MAP, and APMS land-based station in the case of Tehran province, which consists of urban, suburban, and rural levels. The method of research is designed in a time-series manner with the use of Python API, GIS, remote sensing, and various statistics including regression and correlation. All authors read and approved the final manuscript.

Funding

The authors received no financial support for the research, authorship, and publication of this manuscript.

Availability of data and materials

All data generated or analyzed during this research are included in this manuscript.

Competing interests

The authors declare that they have no competing interests.

References

Brunelli, U., Piazza, V., Pignato, L., Sorbello, F., & Vitabile, S. (2007). Two-days ahead prediction of daily maximum concentrations of SO2, O3, PM10, NO2, CO in the urban area of Palermo, Italy. *Atmospheric Environment, 41*(14), 2967-2995. doi:https://doi.org/10.1016/j.atmosenv.2006.12.013

Dareshiri, S., Sahelgozin, M., Lotfian, M., & Ingensand, J. (2019). *Extracting relationship between air pollution and precipitation using spatio-temporal analysis in Tehran metropolis.* Paper presented at the Proc. Int. Cartogr. Assoc. doi:https://doi.org/10.5194/ica-proc-2-23-2019

Feizizadeh, B., & Blaschke, T. (2013). Examining Urban Heat Island Relations to Land Use and Air Pollution: Multiple Endmember Spectral Mixture Analysis for Thermal Remote Sensing. *IEEE Journal of Selected Topics in*

Applied Earth Observations and Remote Sensing, 6(3), 1749-1756. doi:https://doi.org/10.1109/jstars.2013.2263425

Fenger, J. (1999). Urban air quality. *Atmospheric Environment, 33*(29), 4877-4900. doi:https://doi.org/10.1016/S1352-2310(99)00290-3

Flemming, J., Stern, R., & Yamartino, R. J. (2005). A new air quality regime classification scheme for O3, NO2, SO2 and PM10 observations sites. *Atmospheric Environment, 39*(33), 6121-6129. doi:https://doi.org/10.1016/j.atmosenv.2005.06.039

Fu, P., & Weng, Q. (2016). A time series analysis of urbanization induced land use and land cover change and its impact on land surface temperature with Landsat imagery. *Remote Sensing of Environment, 175*, 205-214. doi:https://doi.org/10.1016/j.rse.2015.12.040

Fuladlu, K. (2019). Urban Sprawl Negative Impact: Enkomi Return Phase. *Journal of Contemporary Urban Affairs, 3*(1), 44-51. doi:https://doi.org/10.25034/ijcua.2018.4709

Fuladlu, K. (2020). Urban Sprawl Measurement with Use of VMT Pattern: A Longitudinal Method in Case of Famagusta. *International Journal of Advanced and Applied Sciences, 7*(5), 12-19. doi:https://doi.org/10.21833/ijaas.2020.05.003

Fuladlu, K., Riza, M., & İlkan, M. (2018a). *The Effect of Rapid Urbanization On the Physical Modification of Urban Area.* Paper presented at the The 5th International Conference on Architecture and Built Environment with AWARDs S.ARCH 2018, Venice, Italy.

Fuladlu, K., Riza, M., & İlkan, M. (2018b). *Impact of Urban Sprawl: The Case of the Famagusta, Cyprus.* Paper presented at the 1st Regional Conference: Cyprus Network of Urban Morphology CyNUM 2018, Nicosia, Cyprus.

Jacob, D. J., & Winner, D. A. (2009). Effect of climate change on air quality. *Atmospheric Environment, 43*(1), 51-63. doi:https://doi.org/10.1016/j.atmosenv.2008.09.051

Krotkov, N. A., McLinden, C. A., Li, C., Lamsal, L. N., Celarier, E. A., Marchenko, S. V., . . . Streets, D. G. (2016). Aura OMI observations of regional SO2 and NO2 pollution changes from 2005 to 2015. *Atmos. Chem. Phys., 16*(7), 4605-4629. doi:https://doi.org/10.5194/acp-16-4605-2016

Liu, T., & Yang, X. (2015). Monitoring land changes in an urban area using satellite imagery, GIS and landscape metrics. *Applied Geography, 56*, 42-54. doi:https://doi.org/10.1016/j.apgeog.2014.10.002

Mayer, H. J. (1999). Air pollution in cities. *Atmospheric Environment, 33*(24–25), 4029-4037.

Meng, Z., Ding, G. a., Xu, X., Xu, X., Yu, H., & Wang, S. (2008). Vertical distributions of SO2 and NO2 in the lower atmosphere in Beijing urban areas, China. *Science of The Total Environment, 390*(2), 456-465. doi:https://doi.org/10.1016/j.scitotenv.2007.10.012

Nguyen, M.-V., Park, G.-H., & Lee, B.-K. (2017). Correlation analysis of size-resolved airborne particulate matter with classified meteorological conditions. *Meteorology and Atmospheric Physics, 129*(1), 35-46. doi:https://doi.org/10.1007/s00703-016-0456-y

Owen, T. W., Carlson, T. N., & Gillies, R. R. (1998). An assessment of satellite remotely-sensed land cover parameters in quantitatively describing the climatic effect of urbanization. *International Journal of Remote Sensing, 19*(9), 1663-1681. doi:https://doi.org/10.1080/014311698215171

Richards, J. A., & Jia, X. (1999). *Remote Sensing Digital Image Analysis: An Introduction* (4th ed.). Berlin: Springer-Verlag Berlin Heidelberg.doi:https://doi.org/10.1007/3-540-29711-1.

Ridd, M. K. (1995). Exploring a VIS (vegetation-impervious surface-soil) model for urban ecosystem analysis through remote sensing: comparative anatomy for cities. *International Journal of Remote Sensing, 16*(12), 2165-2185. doi:https://doi.org/10.1080/01431169508954549

Salcedo, R. L. R., Alvim-Ferraz, M. D. C., Alves, C. A., & Martins, F. G. (1999). Time-series analysis of air pollution data. *Atmospheric Environment, 33*(15), 2361-2372. doi:https://doi.org/10.1016/S1352-2310(99)80001-6

Schwartz, J., & Marcus, A. (1990). Mortality and air pollution j london: a time series analysis. *American Journal of Epidemiology, 131*(1), 185-194. doi:https://doi.org/10.1093/oxfordjournals.aje.a115473

Weng, Q. (2001). A remote sensing–GIS evaluation of urban expansion and its impact on surface temperature in the Zhujiang Delta, China. *International Journal of Remote Sensing, 22*(10), 1999-2014. doi:https://doi.org/10.1080/713860788

Weng, Q. (2002). Land use change analysis in the Zhujiang Delta of China using satellite remote sensing, GIS and stochastic modelling. *Journal of Environmental Management, 64*(3), 273-284. doi:https://doi.org/10.1006/jema.2001.0509

Weng, Q. (2009). Thermal infrared remote sensing for urban climate and environmental studies: Methods, applications, and trends. *ISPRS Journal of Photogrammetry and Remote Sensing, 64*(4), 335-344. doi:https://doi.org/10.1016/j.isprsjprs.2009.03.007

Weng, Q., Lu, D., & Schubring, J. (2004). Estimation of land surface temperature–vegetation abundance relationship for urban heat island studies. *Remote Sensing of Environment, 89*(4), 467-483. doi:https://doi.org/10.1016/j.rse.2003.11.005

Weng, Q., & Yang, S. (2006). Urban Air Pollution Patterns, Land Use, and Thermal Landscape: An Examination of the Linkage Using GIS. *Environmental Monitoring and Assessment, 117*(1-3), 463-489. doi:https://doi.org/10.1007/s10661-006-0888-9

Wiederkehr, P., & Yoon, S.-J. (1998). Air quality indicators. In J. Fenger, O. Hertel, & F. Palmgren (Eds.), *Urban Air Pollution - European Aspects* (pp. 403-418). Dordrecht: Springer Netherlands. doi:https://doi.org/10.1007/978-94-015-9080-8

Xue, R., Wang, S., Li, D., Zou, Z., Chan, K. L., Valks, P., . . . Zhou, B. (2020). Spatio-temporal variations in NO2 and SO2 over Shanghai and Chongming Eco-Island measured by Ozone Monitoring Instrument (OMI) during 2008-2017. *Journal of Cleaner Production, 258*, 120563. doi:https://doi.org/10.1016/j.jclepro.2020.120563

Zabalza, J., Ogulei, D., Elustondo, D., Santamaría, J. M., Alastuey, A., Querol, X., & Hopke, P. K. (2007). Study of urban atmospheric pollution in Navarre (Northern Spain). *Environmental Monitoring and Assessment, 134*(1-3), 137-151. doi:https://doi.org/10.1007/s10661-007-9605-6

Zhang, B., Jiao, L., Xu, G., Zhao, S., Tang, X., Zhou, Y., & Gong, C. (2018). Influences of wind and precipitation on different-sized particulate matter concentrations (PM2.5, PM10, PM2.5–10). *Meteorology and Atmospheric Physics, 130*(3), 383-392. doi:https://doi.org/10.1007/s00703-017-0526-9

Figures

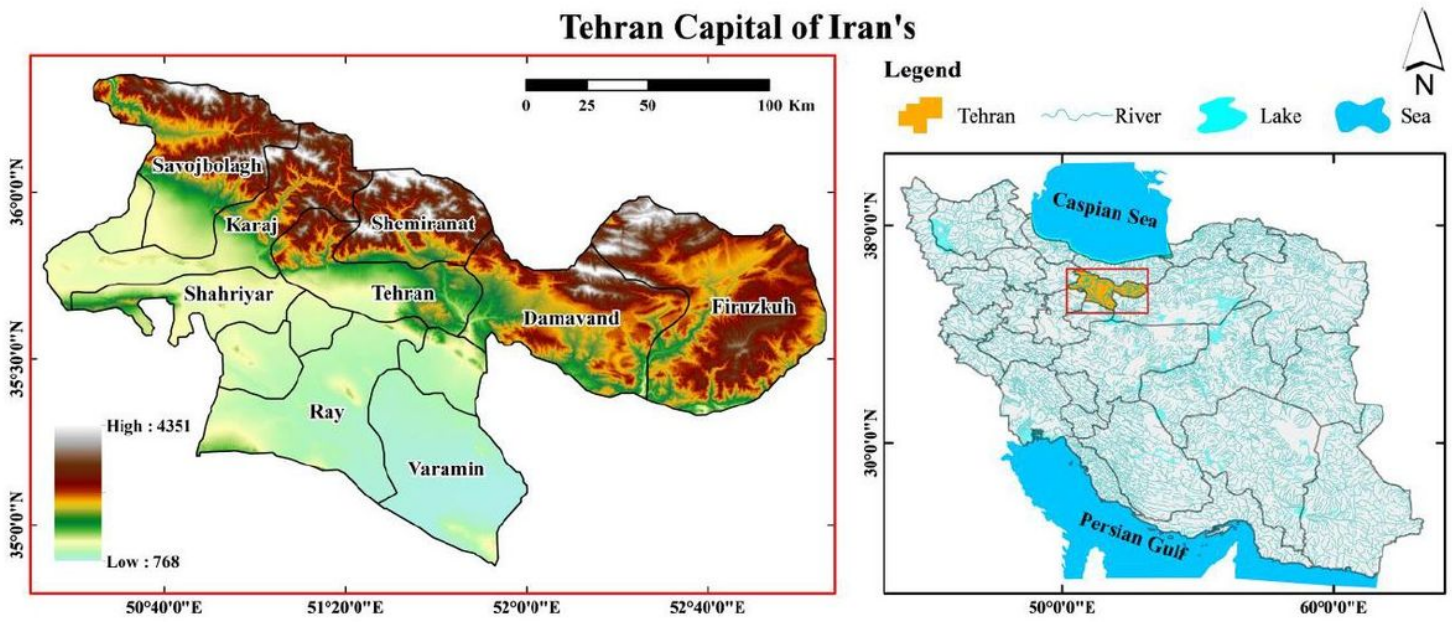

Figure 1

Case Study of Tehran Province DEM (left) Iran (right). Note: The designations employed and the presentation of the material on this map do not imply the expression of any opinion whatsoever on the part of Research Square concerning the legal status of any country, territory, city or area or of its authorities, or concerning the delimitation of its frontiers or boundaries. This map has been provided by the authors.

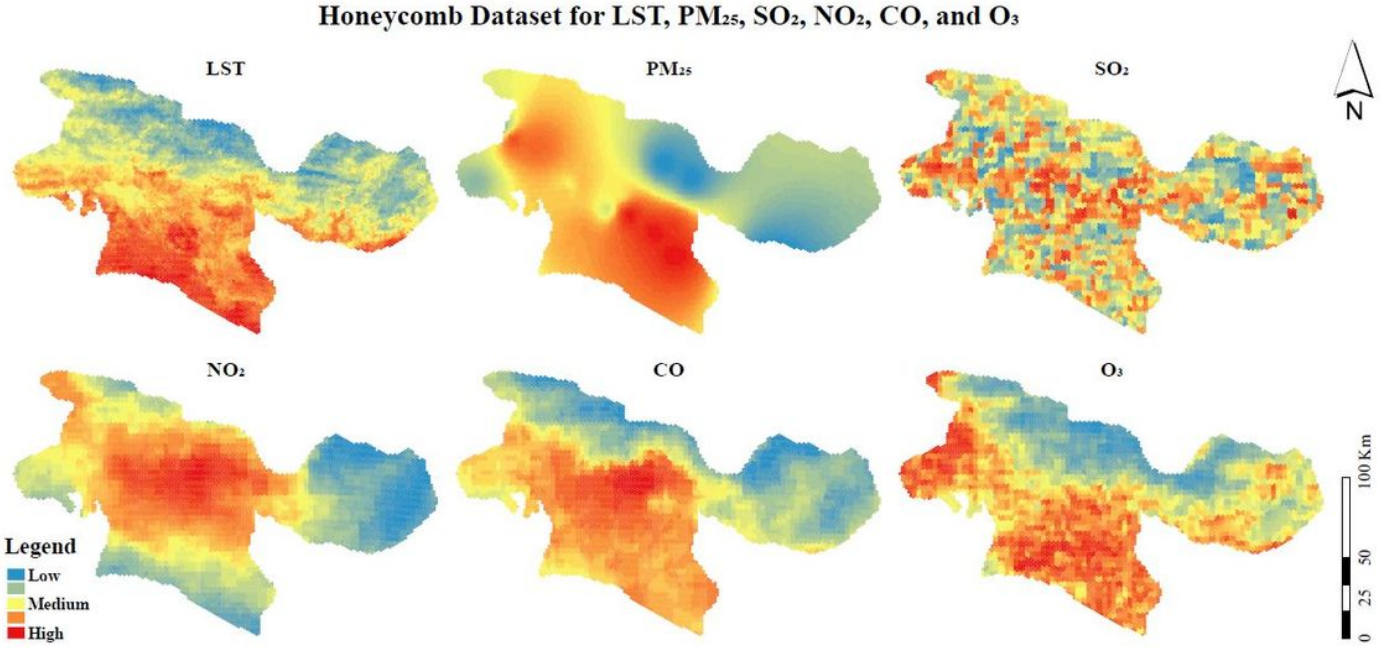

Figure 2

The Classified Honeycomb Attributes for LST, PM□□, SO□, NO□, CO, and O□

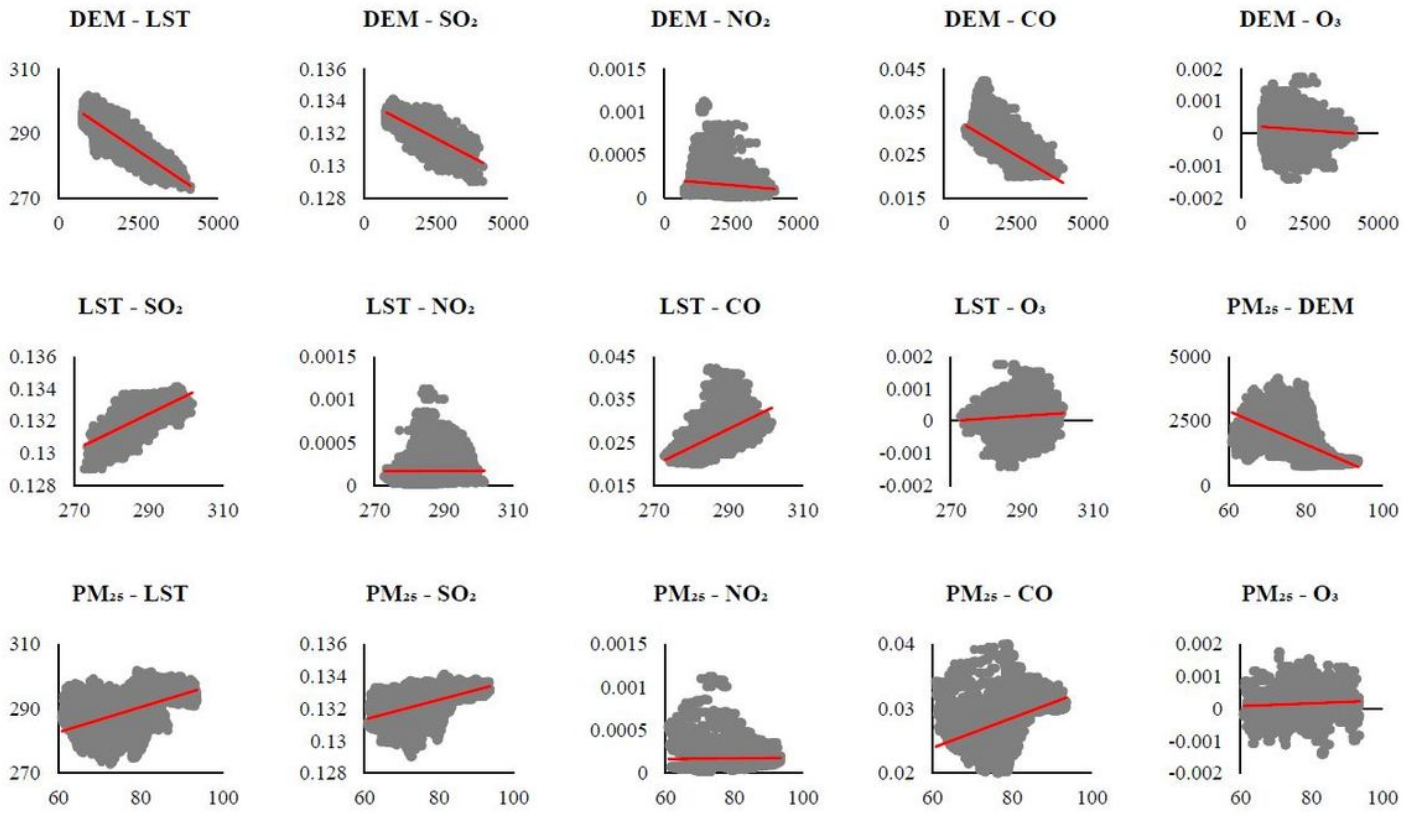

Figure 3

The Scatter-plot among the DEM, LST, PM□□, SO□, NO□, CO, and O□

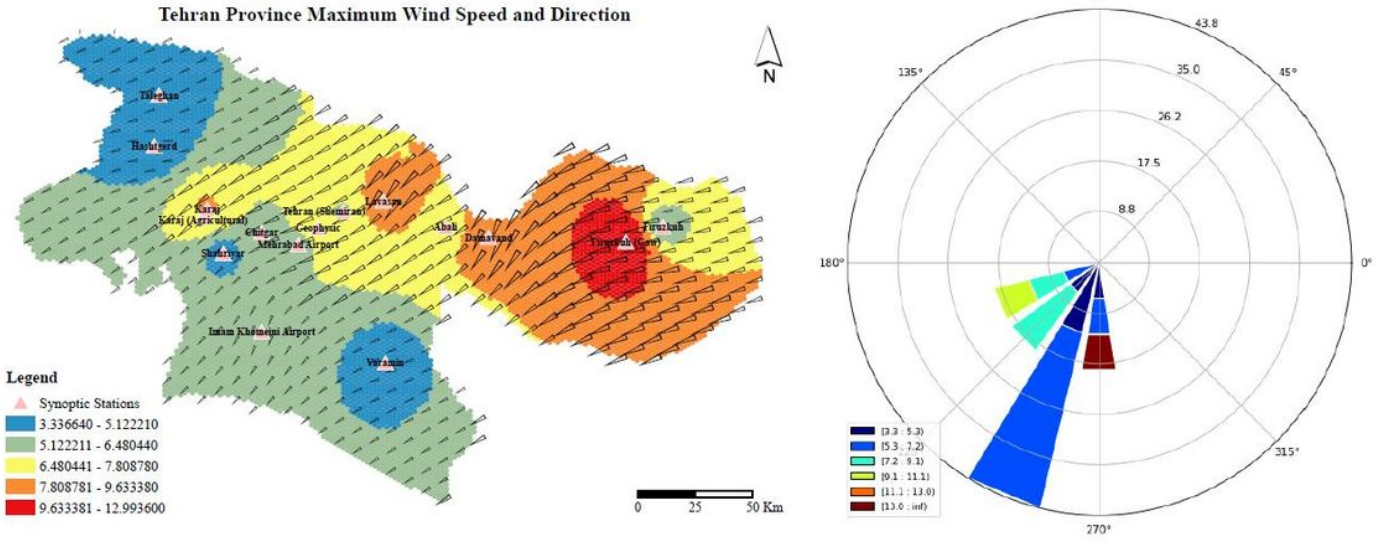

Figure 4

Synoptic Map of Tehran Province (left) Wind-rose diagram (right)

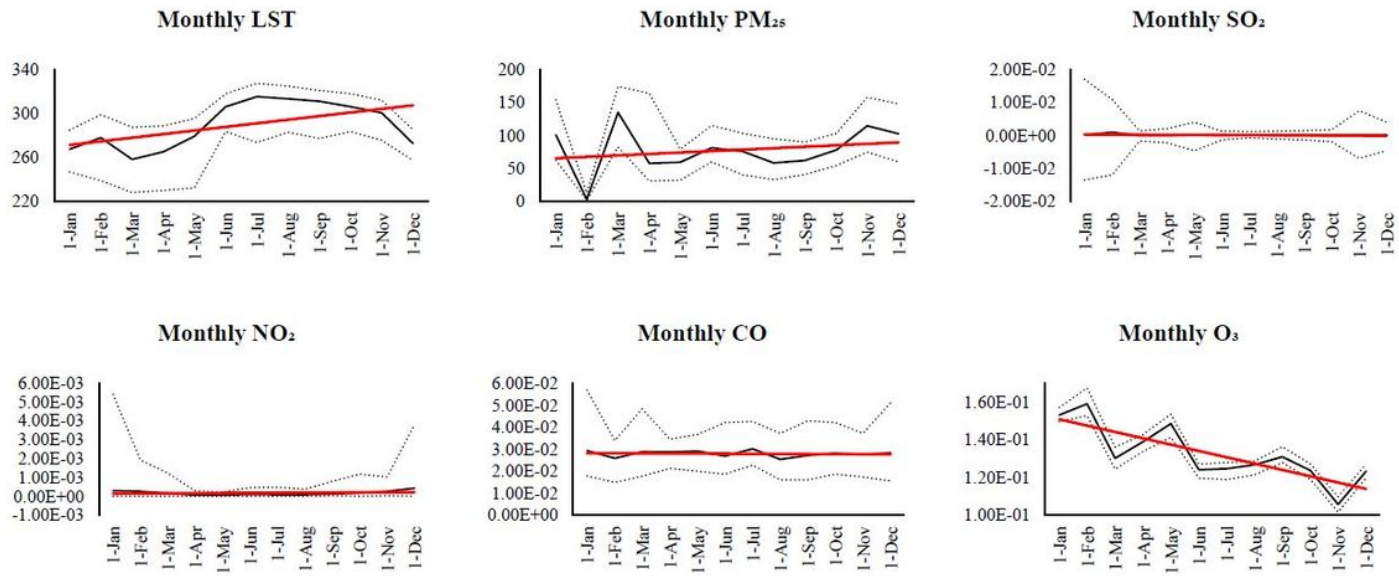

Figure 5

The Monthly Line-plot of the DEM, LST, PM□□, SO□, NO□, CO, and O□